

A vertex-based hierarchical slope limiter for p -adaptive discontinuous Galerkin methods

Dmitri Kuzmin

*Institute of Applied Mathematics (LS III), Dortmund University of Technology
Vogelpothsweg 87, D-44227, Dortmund, Germany*

Abstract

A new approach to slope limiting for discontinuous Galerkin methods on arbitrary meshes is introduced. A local Taylor basis is employed to express the approximate solution in terms of cell averages and derivatives at cell centroids. In contrast to traditional slope limiting techniques, the upper and lower bounds for admissible variations are defined using the maxima/minima of centroid values over the set of elements meeting at a vertex. The correction factors are determined by a vertex-based counterpart of the Barth-Jespersen limiter. The coefficients in the Taylor series expansion are limited in a hierarchical manner starting with the highest-order derivatives. The loss of accuracy at smooth extrema is avoided by taking the maximum of correction factors for derivatives of order $p \geq 1$ and higher. No free parameters, oscillation detectors, or troubled cell markers are involved. Numerical examples are presented for 2D transport problems discretized using a DG method.

Key words: hyperbolic conservation laws, finite elements, discontinuous Galerkin methods, hierarchical bases, slope limiting

1. Introduction

Discontinuous Galerkin (DG) methods [4, 5, 8, 11] represent one of the most promising current trends in computational fluid dynamics. The frequently mentioned advantages of this approach include local conservation and the ease of constructing high-order approximations on unstructured meshes. Moreover, DG methods are well suited for hp -adaptivity and parallelization.

Email address: kuzmin@math.uni-dortmund.de (Dmitri Kuzmin)

Preprint submitted to J. Comput. Appl. Math. (JCAM)

March 19, 2009

One of the major bottlenecks in the design of high-order DG methods for convection-dominated transport problems is the lack of reliable mechanisms that ensure nonlinear stability and effectively suppress spurious oscillations. A number of successful discontinuity capturing and slope limiting techniques are available for DG finite element methods [2, 3, 6, 12, 13, 14, 20] and their finite difference/volume counterparts [1, 19, 22, 21]. However, no universally applicable methodology has been developed to date. Since the accuracy of monotonicity-preserving schemes degenerates to first order at local extrema, free parameters or heuristic indicators are frequently employed to distinguish between troubled cells and regions where the solution varies smoothly. In some cases, the results leave a lot to be desired. Also, the use of limiters may cause severe convergence problems in steady state computations [21].

In the present paper, we devise a parameter-free, non-clipping slope limiter for high-resolution DG-FEM on arbitrary meshes. A hierarchical approach to adaptive p -coarsening is pursued. The Taylor series form [18, 19, 22] of a polynomial shape function is considered, and the involved derivatives are limited so as to control the variations of lower-order terms. The corresponding upper and lower bounds are defined using the data from elements sharing a vertex. This strategy yields a remarkable gain of accuracy, as compared to traditional compact limiters that search the von Neumann (common face) neighbors of a given element [1, 6, 14]. The performance of the new algorithm is illustrated by two-dimensional numerical examples.

2. Upwind DG formulation

A simple model problem that will serve as a vehicle for our presentation of slope-limited DG approximations is the linear convection equation

$$\frac{\partial u}{\partial t} + \nabla \cdot (\mathbf{v}u) = 0 \quad \text{in } \Omega, \quad (1)$$

where $u(\mathbf{x}, t)$ is a scalar quantity transported by a continuous velocity field $\mathbf{v}(\mathbf{x}, t)$. Let \mathbf{n} denote the unit outward normal to the boundary Γ of the domain Ω . The initial and boundary conditions are given by

$$u|_{t=0} = u_0, \quad u|_{\Gamma_{\text{in}}} = g, \quad \Gamma_{\text{in}} = \{\mathbf{x} \in \Gamma \mid \mathbf{v} \cdot \mathbf{n} < 0\}.$$

Multiplying (1) by a sufficiently smooth test function w , integrating over Ω , and using Green's formula, one obtains the following weak formulation

$$\int_{\Omega} \left(w \frac{\partial u}{\partial t} - \nabla w \cdot \mathbf{v}u \right) d\mathbf{x} + \int_{\Gamma} w u \mathbf{v} \cdot \mathbf{n} ds = 0, \quad \forall w. \quad (2)$$

In the discontinuous Galerkin method, the domain Ω is decomposed into a finite number of cells Ω_e , and a local polynomial basis $\{\varphi_j\}$ is employed to define the restriction of the approximate solution $u_h \approx u$ to Ω_e via

$$u_h(\mathbf{x}, t)|_{\Omega_e} = \sum_j u_j(t) \varphi_j(\mathbf{x}), \quad \forall \mathbf{x} \in \Omega_e. \quad (3)$$

The globally defined u_h is piecewise-polynomial and may have jumps at interelement boundaries. The meaning of the coefficients u_j depends on the choice of the basis functions. A local version of (2) can be formulated as

$$\int_{\Omega_e} \left(w_h \frac{\partial u_h}{\partial t} - \nabla w_h \cdot \mathbf{v} u_h \right) d\mathbf{x} + \int_{\Gamma_e} w_h \hat{u}_h \mathbf{v} \cdot \mathbf{n} ds = 0, \quad \forall w_h, \quad (4)$$

where w_h is an arbitrary test function from the DG space spanned by φ_i . Since u_h is multiply defined on Γ_e , the surface integral is calculated using the solution value \hat{u}_h from the upwind side of the interface, that is,

$$\hat{u}_h(\mathbf{x}, t)|_{\Gamma_e} = \begin{cases} \lim_{\delta \rightarrow +0} u_h(\mathbf{x} + \delta \mathbf{n}, t), & \mathbf{v} \cdot \mathbf{n} < 0, \quad \mathbf{x} \in \bar{\Omega} \setminus \Gamma_{\text{in}}, \\ g(\mathbf{x}, t), & \mathbf{v} \cdot \mathbf{n} < 0, \quad \mathbf{x} \in \Gamma_{\text{in}}, \\ \lim_{\delta \rightarrow +0} u_h(\mathbf{x} - \delta \mathbf{n}, t), & \mathbf{v} \cdot \mathbf{n} \geq 0, \quad \mathbf{x} \in \bar{\Omega}. \end{cases} \quad (5)$$

In the case of a piecewise-constant approximation, the result is equivalent to the first-order accurate upwind finite volume scheme. The DG formulation for general conservation laws and systems thereof is described, e.g., in [5, 6].

3. Runge-Kutta DG schemes

Substitution of (3) and (5) into (4) with $w_h = \varphi_i$ yields a system of semi-discrete equations which can be written in matrix form as follows:

$$M \frac{du}{dt} = r(u). \quad (6)$$

Here $u = \{u_j\}$ is the vector of unknown coefficients and $M = \{m_{ij}\}$ is the (block-diagonal) mass matrix. The right-hand side vector $r(u)$ is the contribution of convective terms, including fluxes across the inflow boundary.

The time integration method for the semi-discrete problem (6) should guarantee nonlinear stability, at least for sufficiently small time steps Δt .

Gottlieb and Shu [9] introduced a family of explicit Runge-Kutta methods that preserve the *total variation diminishing* (TVD) property of a 1D space discretization. In general, such time-stepping schemes can be classified as *strong stability-preserving* (SSP) [10]. If the forward Euler method is SSP, so are its high-order counterparts, perhaps under a different restriction on the time step. For details, we refer to the review paper by Gottlieb *et al.* [10].

In this work, we use the optimal third-order SSP Runge-Kutta scheme [9]

$$u^{(1)} = u^n + \Delta t M^{-1} r(u^n), \quad (7)$$

$$u^{(2)} = \frac{3}{4}u^n + \frac{1}{4} [u^{(1)} + \Delta t M^{-1} r(u^{(1)})], \quad (8)$$

$$u^{n+1} = \frac{1}{3}u^n + \frac{2}{3} [u^{(2)} + \Delta t M^{-1} r(u^{(2)})]. \quad (9)$$

Since the DG mass matrix M is block-diagonal, it can be inverted efficiently element-by-element. A time-stepping scheme like (7)–(9) can also be employed as an iterative smoother within the framework of a fast p -multigrid solver [17] in which only coarse-level approximations are treated implicitly.

4. Taylor basis functions

In a discontinuous Galerkin method of degree $p \geq 0$, the shape function $u_h|_{\Omega_e}$ is given by (3), where the number of basis functions depends on p . Clearly, many alternative representations are possible, and some choices are better than others. For accuracy and efficiency reasons, it is worthwhile to consider an orthogonal basis such that M is a diagonal matrix and its inversion is trivial. For example, tensor products of Legendre polynomials are commonly employed on quadrilaterals and hexahedra [2]. The Gram-Schmidt orthonormalization procedure [8, 23], Dubiner’s basis functions [3, 11], and Bernstein-Bézier [7] polynomials are suitable for the construction of hierarchical approximations on triangular meshes. In general, one set of basis functions may be used for matrix assembly and another for limiting or visualization purposes. Due to the local nature of DG methods, conversion between a pair of alternative bases is straightforward and relatively efficient.

Following Luo *et al.* [18], we restrict our discussion to quadratic polynomials $u_h|_{\Omega_e} \in P_2(\Omega_e)$ and consider the 2D Taylor series expansion

$$\begin{aligned} u_h(x, y) = & u_c + \frac{\partial u}{\partial x} \Big|_c (x - x_c) + \frac{\partial u}{\partial y} \Big|_c (y - y_c) + \frac{\partial^2 u}{\partial x^2} \Big|_c \frac{(x - x_c)^2}{2} \\ & + \frac{\partial^2 u}{\partial y^2} \Big|_c \frac{(y - y_c)^2}{2} + \frac{\partial^2 u}{\partial x \partial y} \Big|_c (x - x_c)(y - y_c) \end{aligned} \quad (10)$$

about the centroid (x_c, y_c) of a cell Ω_e . Introducing the volume averages

$$\bar{u}_h = \frac{1}{|\Omega_e|} \int_{\Omega_e} u_h \, d\mathbf{x}, \quad \overline{x^n y^m} = \frac{1}{|\Omega_e|} \int_{\Omega_e} x^n y^m \, d\mathbf{x},$$

the quadratic function u_h can be expressed in the equivalent form [18, 19, 22]

$$\begin{aligned} u_h(x, y) &= \bar{u}_h + \left. \frac{\partial u}{\partial x} \right|_c (x - x_c) + \left. \frac{\partial u}{\partial y} \right|_c (y - y_c) \\ &+ \left. \frac{\partial^2 u}{\partial x^2} \right|_c \left[\frac{(x - x_c)^2}{2} - \overline{\frac{(x - x_c)^2}{2}} \right] + \left. \frac{\partial^2 u}{\partial y^2} \right|_c \left[\frac{(y - y_c)^2}{2} - \overline{\frac{(y - y_c)^2}{2}} \right] \\ &+ \left. \frac{\partial^2 u}{\partial x \partial y} \right|_c \left[(x - x_c)(y - y_c) - \overline{(x - x_c)(y - y_c)} \right]. \end{aligned} \quad (11)$$

This representation has led Luo *et al.* [18] to consider the local Taylor basis

$$\begin{aligned} \varphi_1 &= 1, \quad \varphi_2 = \frac{x - x_c}{\Delta x}, \quad \varphi_3 = \frac{y - y_c}{\Delta y}, \quad \varphi_4 = \frac{(x - x_c)^2}{2\Delta x^2} - \overline{\frac{(x - x_c)^2}{2\Delta x^2}}, \\ \varphi_5 &= \frac{(y - y_c)^2}{2\Delta y^2} - \overline{\frac{(y - y_c)^2}{2\Delta y^2}}, \quad \varphi_6 = \frac{(x - x_c)(y - y_c) - \overline{(x - x_c)(y - y_c)}}{\Delta x \Delta y}. \end{aligned} \quad (12)$$

The scaling by $\Delta x = (x_{\max} - x_{\min})/2$ and $\Delta y = (y_{\max} - y_{\min})/2$ is required to obtain a well-conditioned system [18]. The normalized degrees of freedom are proportional to the cell mean value \bar{u}_h and derivatives of u_h at (x_c, y_c)

$$\begin{aligned} u_h(x, y) &= \bar{u}_h \varphi_1 + \left(\left. \frac{\partial u}{\partial x} \right|_c \Delta x \right) \varphi_2 + \left(\left. \frac{\partial u}{\partial y} \right|_c \Delta y \right) \varphi_3 + \left(\left. \frac{\partial^2 u}{\partial x^2} \right|_c \Delta x^2 \right) \varphi_4 \\ &+ \left(\left. \frac{\partial^2 u}{\partial y^2} \right|_c \Delta y^2 \right) \varphi_5 + \left(\left. \frac{\partial^2 u}{\partial x \partial y} \right|_c \Delta x \Delta y \right) \varphi_6. \end{aligned} \quad (13)$$

Note that the cell averages are decoupled from other degrees of freedom since

$$\int_{\Omega_e} \varphi_1^2 \, d\mathbf{x} = |\Omega_e|, \quad \int_{\Omega_e} \varphi_1 \varphi_j \, d\mathbf{x} = 0, \quad 2 \leq j \leq 6.$$

On a uniform mesh of rectangular elements, the whole Taylor basis (12) is orthogonal, as shown by Cockburn and Shu [6]. On a triangular mesh, this is not the case even for the linear part $\{\varphi_1, \varphi_2, \varphi_3\}$ since the L_2 inner product of φ_2 and φ_3 is nonvanishing. However, the consistent mass matrix M may be ‘lumped’ by setting all off-diagonal entries equal to zero. In contrast to the case of a typical Lagrange basis, this modification is conservative because it does not affect the decoupled equation for the mean value of u_h in Ω_e .

5. The Barth-Jespersen limiter

The above Taylor series representation is amenable to p -adaptation and limiting. In the context of finite volume and DG finite element methods, a slope limiter is a postprocessing filter that constrains a polynomial shape function to stay within certain bounds. Many unstructured grid codes employ the algorithm developed by Barth and Jespersen [1] for piecewise-linear data. Given a cell average $\bar{u}_h = u_c$ and the gradient $(\nabla u)_c$, the goal is to determine the maximum admissible slope for a constrained reconstruction of the form

$$u_h(\mathbf{x}) = u_c + \alpha_e (\nabla u)_c \cdot (\mathbf{x} - \mathbf{x}_c), \quad 0 \leq \alpha_e \leq 1, \quad \mathbf{x} \in \Omega_e. \quad (14)$$

Barth and Jespersen [1] define the correction factor α_e so that the final solution values at a number of control points $\mathbf{x}_i \in \Gamma_e$ are bounded by the maximum and minimum centroid values found in Ω_e or in one of its neighbors Ω_a having a common boundary (edge in 2D, face in 3D) with Ω_e . That is,

$$u_e^{\min} \leq u(\mathbf{x}_i) \leq u_e^{\max}, \quad \forall i. \quad (15)$$

Due to linearity, the solution u_h attains its extrema at the vertices \mathbf{x}_i of the cell Ω_e . To enforce condition (15), the correction factor α_e is defined as [1]

$$\alpha_e = \min_i \begin{cases} \min \left\{ 1, \frac{u_e^{\max} - u_c}{u_i - u_c} \right\}, & \text{if } u_i - u_c > 0, \\ 1, & \text{if } u_i - u_c = 0, \\ \min \left\{ 1, \frac{u_e^{\min} - u_c}{u_i - u_c} \right\}, & \text{if } u_i - u_c < 0, \end{cases} \quad (16)$$

where $u_i = u_c + (\nabla u)_c \cdot (\mathbf{x}_i - \mathbf{x}_c)$ is the unconstrained solution value at \mathbf{x}_i .

The above algorithm belongs to the most popular and successful limiting techniques, although its intrinsic non-differentiability tends to cause severe convergence problems at steady state [19, 21]. Another potential drawback is the elementwise definition of u_e^{\max} and u_e^{\min} which implies that

- the bounds for $u(\mathbf{x}_i)$ satisfying (15) at a vertex \mathbf{x}_i depend on the element number e and may be taken from neighbors that do not contain \mathbf{x}_i ,
- no constraints are imposed on the difference between the solution values in elements meeting at a vertex but having no common edge/face,
- the results are rather sensitive to the geometric properties of the mesh.

In particular, problems are to be expected if Ω_e has sharp angles, as in Fig. 1.

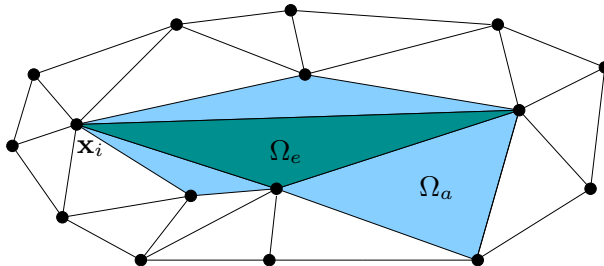


Figure 1: Vertices and neighbors of Ω_e on a triangular mesh.

6. The vertex-based limiter

In light of the above, the accuracy of limited reconstructions can be significantly improved if the bounds for variations $u_i - u_c$ at the vertices of Ω_e are constructed using the maximum and minimum values in the elements containing the vertex \mathbf{x}_i . The so-defined u_i^{\max} and u_i^{\min} may be initialized by a small/large constant and updated in a loop over elements Ω_e as follows:

$$u_i^{\max} := \max\{u_c, u_i^{\max}\}, \quad u_i^{\min} := \min\{u_c, u_i^{\min}\}. \quad (17)$$

The elementwise correction factors α_e for (14) should guarantee that

$$u_i^{\min} \leq u(\mathbf{x}_i) \leq u_i^{\max}, \quad \forall i. \quad (18)$$

This vertex-based condition can be enforced in the same way as (15)

$$\alpha_e = \min_i \begin{cases} \min \left\{ 1, \frac{u_i^{\max} - u_c}{u_i - u_c} \right\}, & \text{if } u_i - u_c > 0, \\ 1, & \text{if } u_i - u_c = 0, \\ \min \left\{ 1, \frac{u_i^{\min} - u_c}{u_i - u_c} \right\}, & \text{if } u_i - u_c < 0. \end{cases} \quad (19)$$

Obviously, the only difference as compared to the classical Barth-Jespersen (BJ) limiter is the use of u_i^{\max} in place of u_e^{\max} . This subtle difference turns out to be the key to achieving high accuracy with p -adaptive DG methods.

In fact, the revised limiting strategy resembles the elementwise version of the finite element flux-corrected transport (FEM-FCT) algorithm developed by Löhner *et al.* [16]. In explicit FCT schemes, u_i^{\max} and u_i^{\min} represent the local extrema of a low-order solution. In accordance with the local discrete maximum principle for unsteady problems, data from the previous time level can also be involved in the estimation of admissible upper/lower bounds.

7. Limiting higher-order terms

The quality of the limiting procedure is particularly important in the case of a high-order DG method [13]. Poor accuracy and/or lack of robustness restrict the practical utility of many parameter-dependent algorithms and heuristic generalizations of limiters tailored for piecewise-linear functions.

Following Yang and Wang [22], we multiply all derivatives of order p by a common correction factor $\alpha_e^{(p)}$. The limited counterpart of (11) becomes

$$\begin{aligned} u_h(x, y) = & \bar{u}_h + \alpha_e^{(1)} \left\{ \frac{\partial u}{\partial x} \Big|_c (x - x_c) + \frac{\partial u}{\partial y} \Big|_c (y - y_c) \right\} \\ & + \alpha_e^{(2)} \left\{ \frac{\partial^2 u}{\partial x^2} \Big|_c \left[\frac{(x-x_c)^2}{2} - \frac{\overline{(x-x_c)^2}}{2} \right] + \frac{\partial^2 u}{\partial y^2} \Big|_c \left[\frac{(y-y_c)^2}{2} - \frac{\overline{(y-y_c)^2}}{2} \right] \right. \\ & \left. + \frac{\partial^2 u}{\partial x \partial y} \Big|_c \left[(x-x_c)(y-y_c) - \overline{(x-x_c)(y-y_c)} \right] \right\}. \end{aligned} \quad (20)$$

In our method, the values of $\alpha_e^{(1)}$ and $\alpha_e^{(2)}$ are determined using the vertex-based or standard BJ limiter, as applied to the linear reconstructions

$$u_x^{(2)}(x, y) = \frac{\partial u}{\partial x} \Big|_c + \alpha_x^{(2)} \left\{ \frac{\partial^2 u}{\partial x^2} \Big|_c (x - x_c) + \frac{\partial^2 u}{\partial x \partial y} \Big|_c (y - y_c) \right\}, \quad (21)$$

$$u_y^{(2)}(x, y) = \frac{\partial u}{\partial y} \Big|_c + \alpha_y^{(2)} \left\{ \frac{\partial^2 u}{\partial x \partial y} \Big|_c (x - x_c) + \frac{\partial^2 u}{\partial y^2} \Big|_c (y - y_c) \right\}, \quad (22)$$

$$u^{(1)}(x, y) = \bar{u}_h + \alpha_e^{(1)} \left\{ \frac{\partial u}{\partial x} \Big|_c (x - x_c) + \frac{\partial u}{\partial y} \Big|_c (y - y_c) \right\}. \quad (23)$$

The last step is identical to (14). In the first and second step, first-order derivatives with respect to x and y are treated in the same way as cell averages, while second-order derivatives represent the gradients to be limited.

Since the mixed second derivative appears in (21) and (22), the correction factor $\alpha_e^{(2)}$ for the limited quadratic reconstruction (20) is defined as

$$\alpha_e^{(2)} = \min\{\alpha_x^{(2)}, \alpha_y^{(2)}\}. \quad (24)$$

The first derivatives are typically smoother and should be limited using

$$\alpha_e^{(1)} := \max\{\alpha_e^{(1)}, \alpha_e^{(2)}\} \quad (25)$$

to avoid the loss of accuracy at smooth extrema. It is important to implement the limiter as a hierarchical p -coarsening algorithm, as opposed to making the

assumption [6] that no oscillations are present in u_h if they are not detected in the linear part. In general, we begin with the highest-order derivatives (cf. [13, 22]) and calculate a nondecreasing sequence of correction factors

$$\alpha_e^{(p)} := \max_{p \leq q} \alpha_e^{(q)}, \quad p \geq 1. \quad (26)$$

As soon as $\alpha_e^{(q)} = 1$ is encountered, no further limiting is required since definition (26) implies that $\alpha_e^{(p)} = 1$ for all $p \leq q$. Remarkably, there is no penalty for using the maximum correction factor. At least for scalar equations, discontinuities are resolved in a sharp and nonoscillatory manner (see below). In the case of hyperbolic systems, the minimum of $\alpha_e^{(p)}$ for the characteristic variables in each coordinate direction (x, y, z) may be taken.

8. Numerical examples

In this section, a preliminary evaluation of the constrained Runge-Kutta DG method is performed on quadrilateral and triangular meshes. For visualization purposes, the approximate solution u_h is projected onto the space V_h of continuous piecewise-linear or bilinear functions via the L_2 projection

$$\int_{\Omega} \tilde{w}_h \tilde{u}_h \, d\mathbf{x} = \sum_e \int_{\Omega_e} \tilde{w}_h u_h \, d\mathbf{x}, \quad \forall \tilde{w}_h \in V_h.$$

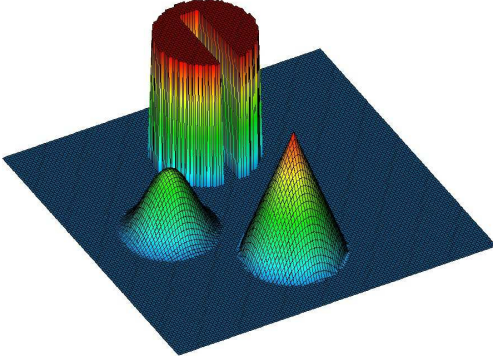
Mass lumping is employed in the current implementation of this postprocessing step which has a smoothing effect. The solution u_h is regarded as nonoscillatory if at least \tilde{u}_h is free of undershoots and overshoots. In practical applications, u_h can be replaced by \tilde{u}_h in equations for other variables.

8.1. Solid body rotation

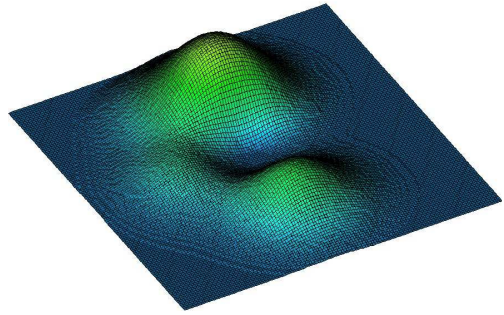
In the first test problem, equation (1) is solved with the incompressible velocity field $\mathbf{v}(x, y) = (0.5 - y, x - 0.5)$ which corresponds to a counterclockwise rotation about the center of the domain $\Omega = (0, 1)^2$. The exact solution reproduces the initial state u_0 exactly after each full revolution ($t = 2\pi k$), so the challenge is to preserve the shape of u_0 as accurately as possible. The initial data shown in Fig. 2a are defined as in [15]. Importantly, not only cell averages but also spatial derivatives are initialized by differentiating u_0 .

Numerical solutions are computed by the Runge-Kutta DG method on a Cartesian mesh with uniform spacing $h = 1/128$. The employed time step is

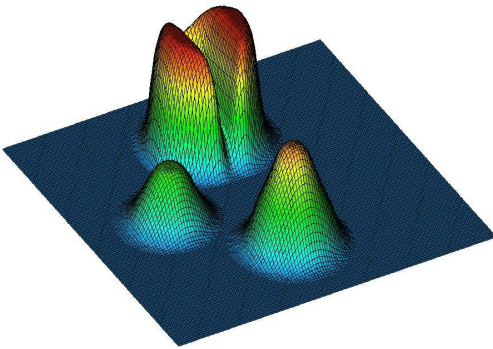
(a) Initial/exact solution, $E_2 = 0.0$



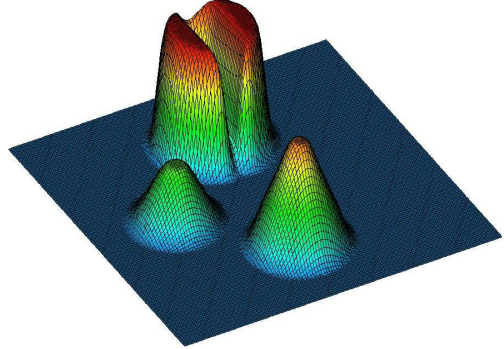
(b) DG- P_0 solution, $E_2=1.80e-1$



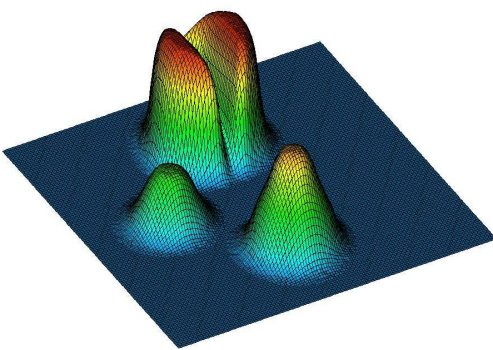
(c) BJ- P_1 solution, $E_2=8.33e-2$



(d) VB- P_1 solution, $E_2=7.19e-2$



(e) BJ- P_2 solution, $E_2=8.51e-2$



(f) VB- P_2 solution, $E_2=6.61e-2$

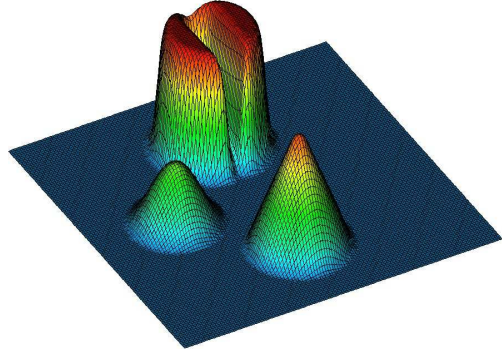
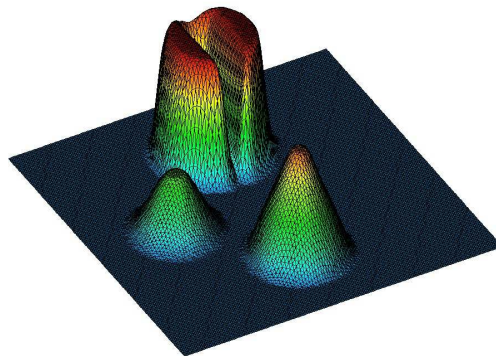
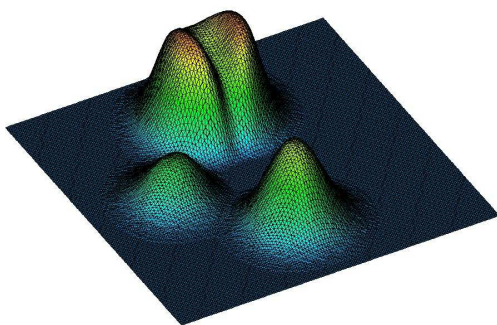


Figure 2: Solid body rotation, simulation on a rectangular mesh, $t = 2\pi$.

$\Delta t = 10^{-3}$. The errors $E_2 = \|u - u_h\|_2$ displayed in Figs. 2–3 are measured in the L_2 norm. The accuracy of the piecewise-constant upwind approximation (DG- P_0 , Fig. 2b) is extremely poor. The piecewise-linear solution produced by the standard Barth-Jespersen limiter (BJ- P_1 , Fig. 2c) is eroded stronger than that obtained with the new, vertex-based approach (VB- P_1 , Fig. 2d). This difference becomes more pronounced in the case of quadratic reconstructions. The BJ- P_2 solution (see Fig. 2e) is still strongly smeared near the two peaks, while the new algorithm (VB- P_2 , Fig. 2f) resolves them with high precision. In both cases, slope limiting was performed hierarchically.

(a) BJ- P_1 solution, $E_2=1.27\text{e-}1$

(b) VB- P_1 solution, $E_2=6.81\text{e-}2$



(c) BJ- P_2 solution, $E_2=1.26\text{e-}1$

(d) VB- P_2 solution, $E_2=6.70\text{e-}2$

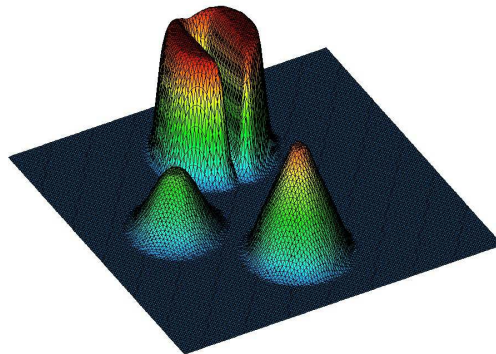
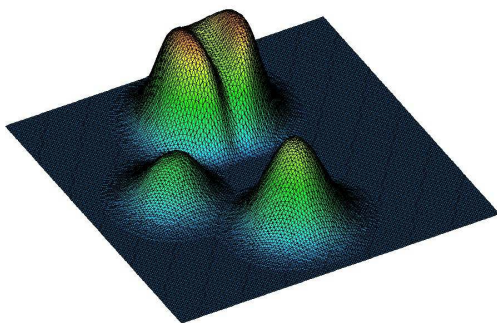


Figure 3: Solid body rotation, simulation on a triangular mesh, $t = 2\pi$.

The results produced by both limiters on a triangular mesh with the same vertices are presented in Fig. 3. In this example, the Taylor basis (12) is not orthogonal. To avoid implicit links between the derivatives to be limited,

all off-diagonal entries of the the mass matrix M were set equal to zero. As explained in section 4, this lumping strategy is conservative. The inclusion of a non-diagonal mass matrix would require the implementation of a limiter for the involved *time* derivatives. The lumped-mass VB solutions (Fig. 3b,d) are comparable to the results in Fig. 2, while the L_2 errors in the BJ solutions (Fig. 3a,c) are twice as large. In this example, searching for local maxima and minima in common face neighbors makes the bounds too restrictive.

8.2. Circular convection

In the second test, the steady-state counterpart of equation (1) is solved in the rectangular domain $\Omega = (0, 2) \times (0, 1)$. The exact solution and inflow boundary conditions for $\mathbf{v}(x, y) = (y, 1 - x)$ are given by the formula

$$u(x, y) = \begin{cases} 1, & \text{if } 0.2 \leq r \leq 0.4, \\ \frac{1}{4} [1 + \cos(\pi \frac{r-0.65}{0.15})], & \text{if } 0.5 \leq r \leq 0.8, \\ 0, & \text{otherwise,} \end{cases} \quad (27)$$

where $r = \sqrt{(x-1)^2 + y^2}$ is the distance from the reference point $(1.0, 0.0)$.

Steady-state solutions are computed using pseudo-time stepping on a uniform rectangular mesh. The mesh size h is the same as before. The constrained P_2 approximations are shown in Fig. 4. Again, the new algorithm delivers superb accuracy and does not smear the cosine hill as it travels along the streamline of the velocity field. Figure 5 demonstrates that the solution profiles at the outflow boundary $\{(x, 0) \mid 1 \leq x \leq 2\}$ are in a good agreement with the exact shape, while the BJ approximation is relatively diffusive.

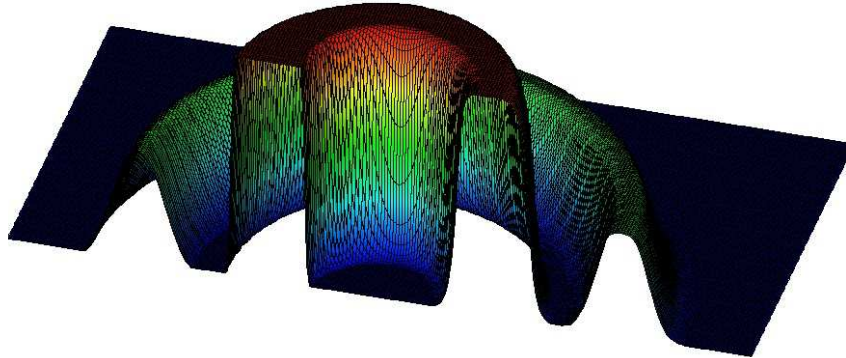
9. Conclusions

This paper sheds some light on the design of generalized slope limiters for high-order discontinuous Galerkin methods. The presented concepts are by no means restricted to the linear convection equation. The embedding into an adaptive hp -FEM framework, implementation of implicit time-stepping schemes, and extension to nonlinear hyperbolic systems seem to be feasible.

References

- [1] T. Barth and D.C. Jespersen, The design and application of upwind schemes on unstructured meshes. *AIAA Paper*, 89-0366, 1989.

(a) BJ- P_2 solution, $E_2=7.43e-2$



(b) VB- P_2 solution, $E_2=6.12e-2$

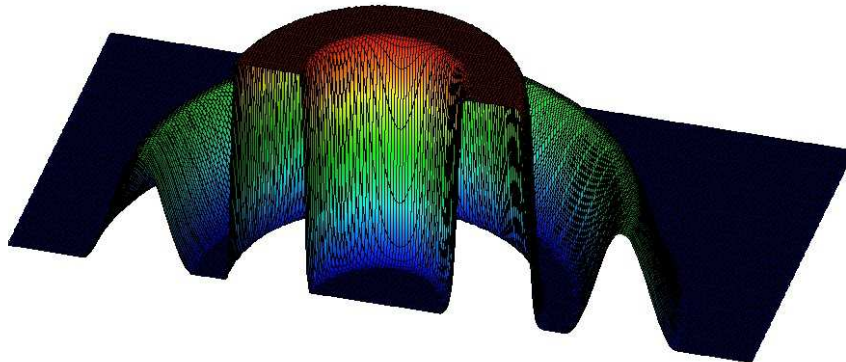


Figure 4: Circular convection, simulation on a rectangular mesh.

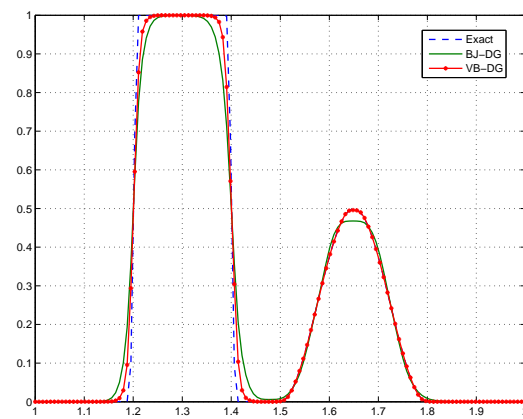


Figure 5: Circular convection, solution profiles at the outlet.

- [2] R. Biswas, K. Devine, and J. E. Flaherty, Parallel adaptive finite element methods for conservation laws. *Appl. Numer. Math.* **14** (1994) 255–284.
- [3] A. Burbeau, P. Sagaut, and C.-H. Bruneau, A problem-independent limiter for high-order Runge-Kutta discontinuous Galerkin methods. *J. Comput. Phys.* **169** (2001) 111–150.
- [4] B. Cockburn, G.E. Karniadakis, and C.-W. Shu, The development of discontinuous Galerkin methods. In: B. Cockburn, G.E. Karniadakis, and C.-W. Shu (eds), *Discontinuous Galerkin Methods. Theory, Computation and Applications*, LNCSE **11** (2000), Springer, New York, 3–50.
- [5] B. Cockburn and C.-W. Shu, Runge-Kutta discontinuous Galerkin methods for convection-dominated problems. *J. Sci. Comput.* **16** (2001) 173–261.
- [6] B. Cockburn and C.-W. Shu, The Runge-Kutta discontinuous Galerkin method for conservation laws V. Multidimensional Systems. *J. Comput. Phys.* **141** (1998) 199–224.
- [7] R.T. Farouki, T.N.T. Goodman, and T. Sauer, Construction of orthogonal bases for polynomials in Bernstein form on triangular and simplex domains. *Computer Aided Geometric Design* **20** (2003) 209–230.
- [8] J.E. Flaherty, L. Krivodonova, J.-F. Remacle, and M.S. Shephard, Aspects of discontinuous Galerkin methods for hyperbolic conservation laws. *Finite Elements in Analysis and Design* **38** (2002) 889–908.
- [9] S. Gottlieb and C.-W. Shu, Total Variation Diminishing Runge-Kutta schemes. *Math. Comp.* **67** (1998) 73–85.
- [10] S. Gottlieb, C.-W. Shu, and E. Tadmor, Strong stability-preserving high-order time discretization methods. *SIAM Review* **43** (2001) 89–112.
- [11] J.S. Hesthaven and T. Warburton, *Nodal Discontinuous Galerkin Methods: Algorithms, Analysis, and Applications*. Springer Texts in Applied Mathematics **54**, Springer, New York, 2008.
- [12] H. Hoteit, Ph. Ackerer, R. Mosé, J. Erhel, and B. Philippe, New two-dimensional slope limiters for discontinuous Galerkin methods on arbitrary meshes. *Int. J. Numer. Meth. Engrg.* **61** (2004) 2566–2593.

- [13] L. Krivodonova, Limiters for high-order discontinuous Galerkin methods. *J. Comput. Phys.* **226** (2007) 879–896.
- [14] L. Krivodonova, J. Xin, J.-F. Remacle, N. Chevaugeon, and J.E. Flaherty, Shock detection and limiting with discontinuous Galerkin methods for hyperbolic conservation laws. *Appl. Numer. Math.* **48** (2004) 323–338.
- [15] R.J. LeVeque, High-resolution conservative algorithms for advection in incompressible flow. *SIAM J. Numer. Anal.* **33** (1996) 627–665.
- [16] R. Löhner, K. Morgan, J. Peraire, and M. Vahdati, Finite element flux-corrected transport (FEM-FCT) for the Euler and Navier-Stokes equations. *Int. J. Numer. Meth. Fluids* **7** (1987) 1093–1109.
- [17] H. Luo, J.D. Baum, and R. Löhner, Fast p -multigrid discontinuous Galerkin method for compressible flows at all speeds. *AIAA Journal* **46** (2008) 635–652.
- [18] H. Luo, J.D. Baum, and R. Löhner, A discontinuous Galerkin method based on a Taylor basis for the compressible flows on arbitrary grids. *J. Comput. Phys.* **227** (2008) 8875–8893.
- [19] K. Michalak and C. Ollivier-Gooch, Limiters for unstructured higher-order accurate solutions of the Euler equations. In: *Proceedings of the AIAA Forty-Sixth Aerospace Sciences Meeting*, 2008.
- [20] S. Tu and S. Aliabadi, A slope limiting procedure in discontinuous Galerkin finite element method for gasdynamics applications. *Int. J. Numer. Anal. Model.* **2** (2005) 163–178.
- [21] V. Venkatakrishnan, Convergence to steady state solutions of the Euler equations on unstructured grids with limiters. *J. Comput. Phys.* **118** (1995) 120–130.
- [22] M. Yang and Z.J. Wang, A parameter-free generalized moment limiter for high-order methods on unstructured grids, AIAA-2009-605.
- [23] M. Zitka, P. Solin, T. Vejchodsky, and F. Avila, Imposing orthogonality to hierarchic higher-order finite elements. *Math. Comput. Simul.* **76** (2007) 211–217.